We study the production of radioisotopes for nuclear medicine in (γ,γ') photoexcitation reactions or $(\gamma, x\mathrm{n}+y\mathrm{p})$ photonuclear reactions for the examples of ^{195m}Pt,^{117m}Sn and ^{44}Ti with high flux $[(10^{13}-10^{15})\gamma/\mathrm{s}]$, small beam diameter and small energy band width $(\Delta E/E \approx 10^{-3}-10^{-4})$ γ beams. In order to realize an optimum γ-focal spot, a refractive γ-lens consisting of a stack of many concave micro-lenses will be used. It allows for the production of a high specific activity and the use of enriched isotopes. For photonuclear reactions with a narrow γ beam, the energy deposition in the target can be reduced by using a stack of thin target wires, hence avoiding direct stopping of the Compton electrons and e^+e^- pairs. The well-defined initial excitation energy of the compound nucleus leads to a small number of reaction channels and enables new combinations of target isotope and final radioisotope. The narrow-bandwidth γ excitation may make use of collective resonances in γ-width, leading to increased cross sections. (γ,γ') isomer production via specially selected γ cascades allows to produce high specific activity in multiple excitations, where no back-pumping of the isomer to the ground state occurs. The produced isotopes will open the way for completely new clinical applications of radioisotopes. For example ^{195m}Pt could be used to verify the patient's response to chemotherapy with platinum compounds before a complete treatment is performed. In targeted radionuclide therapy the short-range Auger and conversion electrons of ^{195m}Pt and ^{117m}Sn enable a very local treatment. The generator ^{44}Ti allows for a PET with an additional γ-quantum (γ-PET), resulting in a reduced dose or better spatial resolution.

Keywords: Gamma-ray sources, Photonuclear reactions, Radioactive sources for therapy, Nuclear medicine imaging, Radiopharmaceuticals, Gamma-ray lens

1. INTRODUCTION

This publication is intended to focus in more detail on three medical radioisotopes ^{195m}Pt, ^{117m}Sn and ^{44}Ti, while the more general concepts of medical radioisotope production with brilliant γ-beams have been introduced in Ref.[1] In nuclear medicine radioisotopes are used for diagnostic and therapeutic purposes.[2,3] Many diagnostics applications are based on molecular imaging methods, i.e. either on positron emitters for 3D imaging with PET (positron emission tomography) or gamma ray emitters for 2D imaging with planar gamma cameras or 3D imaging with SPECT (single-photon emission computer tomography)*. The main advantage of nuclear medicine methods is the high sensitivity of the detection systems that allows using tracers at extremely low concentrations. This extremely low amount of radiotracers assures that they do not show any (bio-)chemical effect on the organism. Thus, the diagnostic procedure does not interfere with the normal body functions and provides direct information on them, not perturbed by the detection method. To maintain these intrinsic advantages of nuclear medicine diagnostics, one has to assure that radiotracers of *relatively high specific activity* are used, i.e. that the injected radiotracer is not accompanied by too many stable isotopes of the same (or a chemically similar) element.

Radioisotopes are also used for therapeutic applications, in particular for endo-radiotherapy. Targeted systemic therapies allow fighting diseases that are non-localized, e.g. leukemia and other cancer types in an advanced

state, when already multiple metastases have been created. Usually a bioconjugate[2,6] is used that shows a high affinity and selectivity to bind to peptide receptors or antigens that are overexpressed on certain cancer cells with respect to normal cells. Combining such a bioconjugate with a suitable radioisotope, such as a low-energy electron emitter, allows irradiating and destroying selectively the cancer cells. Depending on the nature of the bioconjugate, these therapies are called Peptide Receptor Radio Therapy (PRRT)[3,4] when peptides are used as bioconjugates or radioimmunotherapy (RIT),[3,5] when antibodies are used as bioconjugates. The radioisotopes for labeling of the bioconjugates should have a high specific activity to minimize injection of bioconjugates labeled with stable isotopes that do not show radiotherapeutic efficiency. Thus again *high specific activities* are required for radioisotopes used in such therapies. In the cases of ^{195m}Pt and ^{117m}Sn for radiotherapeutic applications a low-energy γ transition can be used for SPEC imaging.

The long-lived ^{44}Ti isotope ($T_{1/2} \approx 60$a) will be used as a generator to produce the shorter-lived ^{44}Sc ($T_{1/2}$= 4 h), which has the unique property to populate predominantly the first excited 1157 keV state in ^{44}Ca. Thus the e^+ annihilation into two counterpropagating 511 keV γ-quanta is accompanied by the third prompt γ transition of 1157 keV, allowing a unique localization of each individual decay.[25] Previously already one ^{44}Ti generator has been produced via the ^{44}Sc(p,2n) reaction in an irradiation for several months. All the development of the ^{44}Ti/^{44}Sc generator and the medical application of ^{44}Sc to patients have been established.[22,23]

The radioisotopes for diagnostic or therapeutic nuclear medicine applications are usually produced by nuclear reactions. The required projectiles are typically either neutrons from dedicated reactors or charged particles from cyclotrons or other accelerators. In our publication[1] we have compared these methods in detail to a production scheme using a γ-beam and discussed a large variety of new possible radioisotopes produced by γ-beams. In section 2 we describe the most recent developments on brilliant γ-beams. In section 3 we describe a γ lens, with which the specific activity can be increased by optimum focusing at the production target. While the γ facilities allow to produce many radioisotopes in new photonuclear reactions with significantly higher specific activity, we here focus on the three radioisotopes ^{195m}Pt, ^{117m}Sn and ^{44}Ti. In section 4 we discuss these special cases.

2. HIGHLY BRILLIANT γ SOURCES

The new γ beams are produced via Compton back-scattering of laser photons from a relativistic electron beam. The presently world-leading facility for photonuclear physics is the High-Intensity γ-ray Source (HIγS) at Duke University (USA). It uses the Compton back-scattering of photons, provided by a high-intensity Free-Electron Laser (FEL), in order to produce a brilliant γ beam. The γ intensity in the energy range between 1 MeV and 160 MeV amounts to $10^8 s^{-1}$ with a band width of about 5%.[11] The brilliant Mono-Energetic Gamma-ray (MEGa-ray) facility at Lawrence Livermore National Laboratory (USA) is based on a normal-conducting electron linac and will yield already in 2012 for γ energies between 0.5 and 2.5 MeV a γ intensity of $10^{13} s^{-1}$ with an energy band width of down to 10^{-3} and a brilliance of $10^{22}/[mm^2 mrad^2 s 0.1\% BW]$.[12] Using the same accelerator technology, at the upcoming Extreme Light Infrastructure - Nuclear Physics (ELI-NP) facility in Bucharest, until 2015 a γ beam will become available, providing about the same γ intensity and band width in the energy range of 1-19 MeV.[13]

At present, great efforts are also invested all over the world to realize highly brilliant γ beams based on the Energy Recovery Linac (ERL) technology. The Energy Recovery Linac (ERL) requires a new type of superconducting electron accelerator that provides a highly brilliant, high-intensity electron beam. The main components of an ERL are an electron injector, a superconducting linac, and an energy recovery loop. After injection from a highly brilliant electron source, the electrons are accelerated by the time-varying radio-frequency field of the superconducting linac. The electron bunches are transported once through a recirculation loop and are re-injected into the linac during the decelerating RF phase of the superconducting cavities. So the beam dump has to take the electron bunches only with low energy, while the main part of the electron energy is recycled. At ERL's, high-energy, highly brilliant γ beams can be created by Compton back-scattering of photons with high energy (0.1-100 MeV), again recirculating the photons in a very high finesse cavity with MW power to overcome the small Compton cross section. ERL technology is pioneered at Cornell University (together with Thomas Jefferson National Laboratory),[16–18] where an ERL is presently constructed for a 5 GeV, 100 mA electron beam. At the KEK accelerator facility in Japan, an ERL project is presently pursued aiming at a γ beam with an intensity of $10^{13} s^{-1}$.[14,15] In Germany, a high-current and low-emittance demonstrator ERL facility (BERLinPro) is

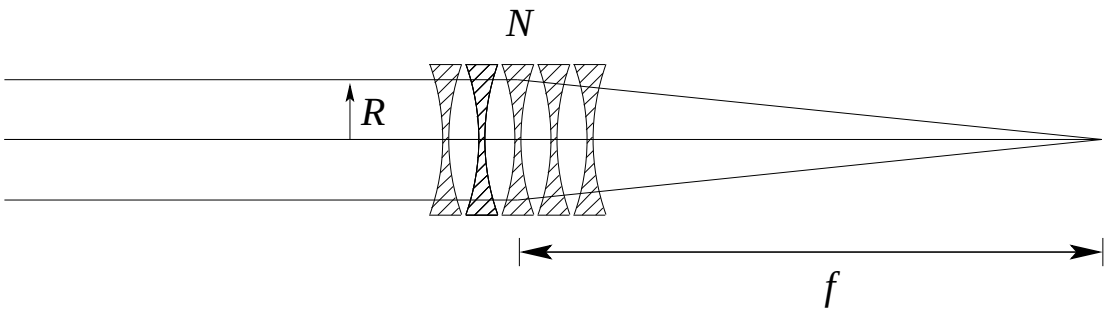

Figure 1. γ-lens consisting of N micro-lenses, irradiated with a γ-beam of radius R. The γ lens has a focal length f.

developed at the Helmholtz Zentrum Berlin.[19] There are mainly three different operation modes of an ERL: high-flux mode, high-brilliance mode, and a short-pulse mode.[15–17] For our purpose of medical isotope production the high brilliance mode is of particular interest. The ultimately envisaged photon intensity is $> 10^{15} s^{-1}$ in an energy range of 0.5 - 25 MeV. Such a facility would provide a brilliant pulsed (ps pulse length) γ beam with a narrow band width of about $< 10^{-3}$, and a low emittance of $10^{-4} mm^2 mrad^2$.

3. γ LENS WITH MONOCHROMATISATION

Lenses for hard X-rays are well established[7–10] for energies up to 200 keV. At synchrotrons the brilliance decreases more than exponential above 100 keV energies. Here we want to extend the range of these lenses to MeV-γ-beams, making use of their many orders of magnitude higher brilliance. Since the real part δ of the index of refraction $n = 1 - \delta + i\beta$ decreases with $1/E_\gamma^2$, the realization of sufficent focusing strength becomes more difficult. On the other hand, the imaginary part β of the index of refraction decreases even faster with $1/E_\gamma^{3.5}$. At higher energies new processes like Compton scattering and pair creation contribute to β. Only with the new highly brilliant γ-beams the smaller beam radius R allows to reach reasonable focal lengths f. A further trick to reduce the focal length is to stack a larger number N of micro-lenses behind each other. The focal length f is given by

$$f = \frac{R}{2\delta N} \tag{1}$$

For the real part δ of the index of refraction we have:

$$\delta = \frac{r_e \lambda_\gamma^2}{2\pi} \rho \frac{Z}{A} \propto \frac{1}{E_\gamma^2} \tag{2}$$

Here r_e is the classical electron radius, $\lambda_\gamma = \frac{\hbar c}{E_\gamma}$ is the γ wavelength, ρ is the lens density and Z and A are the charge and mass number of the lens material, respectively. Since the real part δ of the index of refraction is negative for γ-energies, we show concave lenses in Fig. 1.

We now have to consider the special case that we will use in combination with the γ-lens always γ-beams produced by Compton back-scattering from relativistic electrons. Here the γ-energy E_γ is given by:

$$E_\gamma = \frac{2\gamma_e^2 \cdot (1 + \cos\phi) \cdot E_L}{1 + (\gamma_e \Theta)^2 + \frac{4\gamma_e E_L}{m_e c^2}} \tag{3}$$

E_L is energy of the primary laser photons, $\gamma_e = \frac{E_e}{m_e c^2}$ is the γ-factor of the electron beam with energy E_e and the electron rest mass m_e and we consider that the laser beam enters under an angle ϕ with respect to the electron direction and the outcoming γ photon has an angle Θ with respect to the electron beam direction. Thus for $\Theta = 1/\gamma_e$ the emitted γ photon has about a factor of 2 smaller γ-energy that the γ-photon in electron beam direction. For angles $\Theta_{BW} \leq \frac{\sqrt{BW}}{\gamma_e}$, the central γ beam opening cone, it is no longer the Θ dependance of the

Compton scattering, but other factors like the band width of the electron beam or the band width of the laser beam, which determine the band width BW of the γ-beam. We will now limit the acceptance angle of the γ lens or the corresponding γ beam radius R at the entrace to the lens to this much smaller angle Θ_{BW}, where furthermore the main intensity of the γ beam is concentrated. Thus we make use of the very special γ energy angle correlation of Compton backscattered γ rays to work with a very small radius R and to obtain a natural monochromatisation. The outer angles Θ are no longer focused by the lens. We can experimentally monitor the energy range focused by the lens by using a special nuclear resonance γ energy and measure the nuclear resonance fluorescence (NRF) for a thin wire target, probing the γ beam focus behind the γ lens. The better the band width of the central γ beam the smaller the radius R and the focal length f will be. For higher γ beam energies and correspondingly larger γ_e the radius R will be smaller, partially compensating the strong γ energy dependance of the focal length f with $\propto \frac{1}{E_\gamma^2} \propto \frac{1}{\gamma_e^4}$. By increasing the number N of micro-lenses and using materials of higher density ρ, we can keep the focal length sufficiently small for γ beams with sufficiently good primary band width BW. In the very central region the very thin micro-lenses will lead to small absortion of the γ beam. We have to align the γ lens very accurately with respect to the electron beam direction, but again this can be monitored by NRF measurements.

When reducing the γ beam radius along the stack of lenses, the shape of the lenses can be adjusted adiabatically and very small focal spots can be reached.[7] For our production of medical radioisotopes we want to reach a very small spot size on the target to obtain higher specific activity and to allow for the use of isotopically enriched targets. The small diameter wire-targets allow for an easy escape of Compton electrons and pairs, resulting in little heating.

4. SPECIAL RADIOISOTOPES

4.1 The nuclei ^{195}Pt and ^{117}Sn

^{195}Pt and ^{117,119}Sn have many common properties. ^{195}Pt has above its $1/2^-[530]$ Nilsson ground state a $13/2^+[606]$ isomer at 259 keV with a halflife of 4 d. The isomer originates from the $1i_{13/2}$ intruder state from the next higher shell. For the semi-magic ^{117,119}Sn with Z=50, the situation is very similar to ^{195}Pt, except that all angular momenta and the main shell quantum number are reduced by one. Thus the intruder $1i_{13/2}$ state of ^{195}Pt is replaced by the intruder $1h_{11/2}$ state for ^{117}Sn. The ground state $1/2^+[404]$ of ^{117,119}Sn originates from a $2d_{3/2}$ state. The $11/2^-$ isomer at 315 keV of ^{117}Sn originates from the $1h_{11/2}$ neutron state and has a half-life of $T_{1/2}$= 13.6 d. The corresponding $11/2^-$ isomer of ^{119}Sn at 89.5 keV has a half-life of $T_{1/2}$=293 d, which is too long for medical applications.

But also the neighbouring even-even nuclei have many similarities. The Pt nuclei have close-lying shell model states with $\Delta N = 1, \Delta l = \Delta j = 3$,[20,21] here the $i_{13/2}$ and $f_{7/2}$ states, which lead to octupole deformation and low-lying collective 3^- states. These 3^- octupole states are coupled to 2^+ quadrupole states, resulting in collective 1^- states. One could also couple a collective 5^- and 4^+ to a collective 1^- state. These 1^- states have rather large dipole moments of about 0.1 e fm. The 5^- state may be due to shell model states with an angular momentum difference $\Delta l = \Delta j = 5$ of the $i_{13/2}$ and $p_{3/2}$ states. In this way one could explain the strong E1 core excitation and its strong collective core deexcitation by a $1^- \rightarrow 3^- \rightarrow 5^-$ cascade with collective E2 transitions. The 5^- core excitation then will decay predominantly to the $i^+_{13/2}$ state. The f and p shell-model states lying close to the i shell-model state explain the collective $3^-, 5^-$ core excitations in the neighbouring ^{194,196}Pt isotopes. Also on top of the $13/2^-$ isomer low-lying collective quadrupole excitations exist, which will mix with the high-spin states of the core 3^- and 5^- excitations and the $1/2^+$ ground state, leading to the strong cascade coupling the gateway state with the 1^- core excitation to the high spin isomer.

Also for the Sn nuclei we have close-lying shell-model states with $\Delta N = 1, \Delta l = \Delta J = 3$ to explain the strong octupole state and by coupling to the 2^+ quadrupole state the dipole E1 transition.[21]

We can extrapolate all these collective states of neighbouring even-even nuclei to the odd-neutron ^{195}Pt and ^{117}Sn. We verify a weak coupling of the core excitations for known collective states in these odd nuclei. Thus we predict a $1/2^+$ and $3/2^+$ E1 excitation from the $1/2^-$ ground state to the 1^- core excitation at about 1.8 MeV for ^{195}Pt and a $1/2^-$ and $3/2^-$ E1 core excitation from the ground state of ^{117}Sn at about 3.8 MeV.

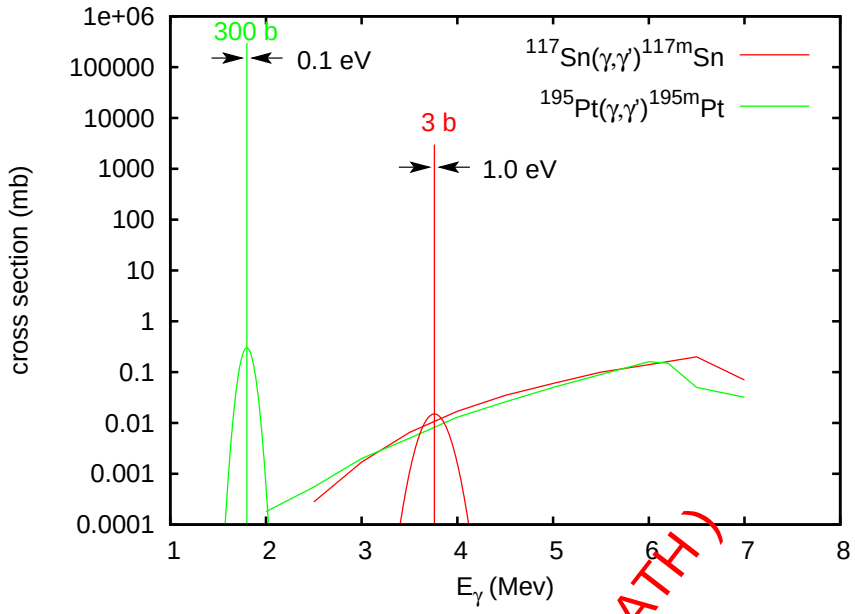

Figure 2. Statistical model calculation for the cross section with the TALYS code, giving the broad cross-section dependence and predicted additional collective resonances deduced from neighbouring even-even nuclei.

4.1.1 Production of the Isomers ^{195m}Pt and ^{117m}Sn

In Fig. 2 we show the predicted photonuclear cross-sections as a function of γ-energy. Besides the statistical calculations with the TALYS code and standard parameters, we show the new expected collective gateway states. Their relative yield has to be adjusted to reproduce the integrated yields. At present for ^{195}Pt and ^{117}Sn only one survey experiment including 19 nuclides exists, where the integrated cross section $\sigma \cdot \Gamma$ was deduced for one bremsstrahlung spectrum ranging from 0.5 MeV to 4 MeV and another one ranging from 1.0 MeV to 6 MeV. A *"three to four orders of magnitude larger integrated cross section than usually"* was observed including ^{195m}Pt and ^{117m}Sn.[28] In the analysis one single gateway state at 2.125 MeV was artificially introduced for all 19 nuclides, when deducing the effective $\sigma \cdot \Gamma$. We now want to perform at HIγS a search for these individual resonant gateway states for ^{195}Pt and ^{117}Sn. Then we could localize them more accurately with the better band width of the MEGa-ray or ELI-NP facilities. These resonances would facilitate the photonuclear production of these isomers significantly.

4.1.2 Medical Applications of ^{195m}Pt and ^{117m}Sn

^{195m}Pt: Determining the efficiency of chemotherapy for tumors and the optimum dose by nuclear imaging In chemotherapy of tumors most often platinum cytotoxic compounds like cisplatin or carbonplatin are used. We want to label these compounds with ^{195m}Pt for pharmacokinetic studies like tumor uptake and want to exclude "nonresponding" patients from unnecessary chemotherapy and optimizing the dose of all chemotherapy. For such a diagnostics a large-scale market can be foreseen, but it would also save many people from painful treatments. We estimated in Ref.[1] that several hundred patient-specific uptake samples per day could be produced with a γ beam facility if optimum gateway states are identified by scanning the isomer production with high γ beam resolution. ^{195m}Pt has a high $13/2^+$ spin isomer at 259 keV, halflife ($T_{1/2}$= 4 d) with SPECT transitions of 130 keV and 99 keV to the $1/2^-$ ground state.

^{195m}Pt: Cancer Therapy with Short-Range Electrons On the other hand, ^{195m}Pt may be used in cancer therapy by transporting it to the tumor by specific bioconjugates.[29] Special antibodies may be used in radio-imunotherapy (RIT) or special peptides in Peptide Receptor Radionuclide therapy (PRRT) to guide the radioactive isotope to the tumor. In Fig. 3 we show how a radionuclide like ^{195m}Pt is transported with a chelator to the specific peptide receptor.

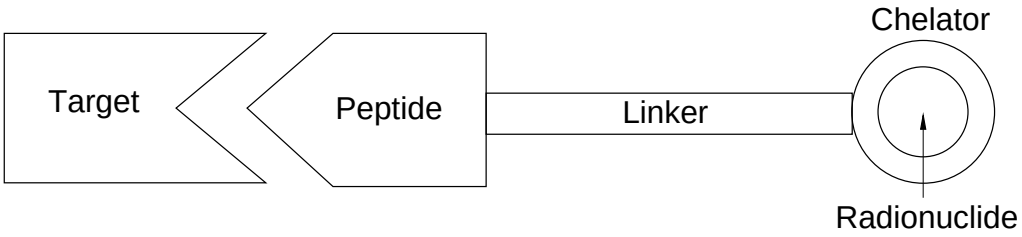

Figure 3. Schematic picture explaining how a specific radionuclide can be transported to a specific petide receptor.

Here ^{195m}Pt is of high interest, because the emitted conversion electrons and Auger electrons have a rather small range of 1.5-200 μm and low electron energies of 7 keV, 17 keV, 21 keV and 116 keV, respectively. They allow to kill locally small tumor clusters, while the dose given to normal tissue is rather low. Several new therapeutic radioisotopes with this small range and high LET can be produced by γ beams.

^{117m}Sn An emitter of low energy Auger electrons for tumor therapy Auger electron therapy requires targeting into individual tumor cells, even into the nucleus or to DNA, due to the short range below 1μm of the Auger electrons; but there it is of high REB due to the shower of the abundantly produced 5-30 Auger electrons.[32] On the other hand, Auger radiation is of low toxicity, while being transported through the body. Thus Auger electron therapy[30] needs special tumor-specific transport molecules like antibodies or peptides. Many of the low-lying high spin isomers produced in (γ,γ') reactions have strongly converted transitions, which trigger these large showers of Auger cascades.

Once the optimum production of the isomers ^{195m}Pt and ^{117m}Sn has been established, the scientific focus will shift to produce the best bioconjugates to transport these radioisotopes to specific cancer cells.

4.2 The Generator ^{44}Ti

4.2.1 Photoproduction of ^{44}Ti

In the α-cluster model, ^{46}Ti and ^{44}Ti have a simple structure. Both nuclei have a strongly bound doubly magic ^{40}Ca core, which in the α-cluster model consists of 10 α particles forming the spherical core. For ^{44}Ti we add an additional α particle to the doubly magic ^{40}Ca core, obtaining a deformed nucleus. ^{46}Ti can be obtained by adding two valence neutrons to the ^{44}Ti. This structure is shown in Fig. 4.

The very strongly bound α particles make it probable that we obtain two loosely bound halo neutrons when we photo-excite ^{46}Ti, such that it can emit just two low-energy neutrons. Since these halo neutrons result in large dipole monents and strong E1 excitations, we expect strong collective resonances close to the reaction threshold. We expect a deformation splitting with a deformation of ^{46}Ti of about $\beta = 0.3$, resulting in a high-energy component $E_{GDR\perp} = E_{GDR} \cdot (1 + \beta/3)$, corresponding to about 24.1 MeV, and a low-energy component $E_{GDRz} = E_{GDR} \cdot (1 - \beta \cdot (2/3))$, corresponding to about 17.5 MeV. This GDR is shown in Fig. 5 with its splitting due to the quadrupole deformation into a high-energy component $E_{GDR\perp}$ with an oscillation normal to the z

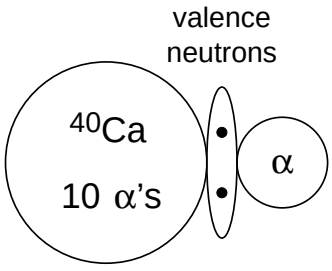

Figure 4. α-cluster model of ^{46}Ti.

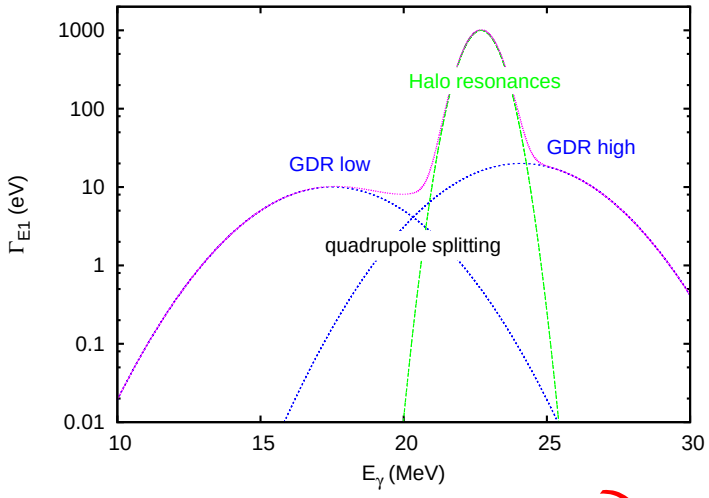

Figure 5. Schematic E1 strength of ^{46}Ti. The γ width of about 1.3 eV at 13.2 MeV is confirmed in Ref.[33]

axis, and a component half as strong at E_{GDRz} along the z axis. Microscopically, in the E1 excitation we have to lift up two 1f7/2 neutrons to form 1^- states. Thus we will have $3s_{1/2}$ neutron levels populated close to zero binding energy, but also some odd angular momentum states. These weakly bound states will decay sequencially into two neutrons above the 2n-threshold, but due to the s-neutron components in the wavefunctions they will have extended wave functions and an enhanced E1 strength.

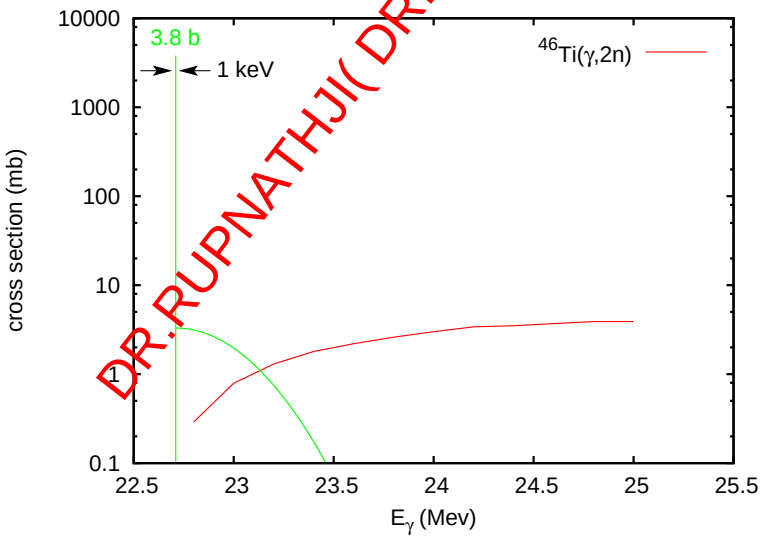

Figure 6. Cross section for the ^{46}Ti$(\gamma, 2n)^{44}$Ti reaction calculated with the TALYS code. Also shown is a halo resonance at the reaction threshold.

In Fig. 6 we show in red the usual energy dependence of the ^{46}Ti(γ,2n)^{44}Ti cross section from statistical model simulations with the code TALYS. In addition we hope to find this predicted strong new resonance.

4.2.2 A $^{44}Ti \rightarrow ^{44}$Sc generator for the γ-PET isotope

In recent years PET (Positron Emission Tomography) with a typical spatial resolution of 3-10 mm was supplemented by multi-slice X-ray CT (Computer Tomography) of much better resolution, leading to the novel

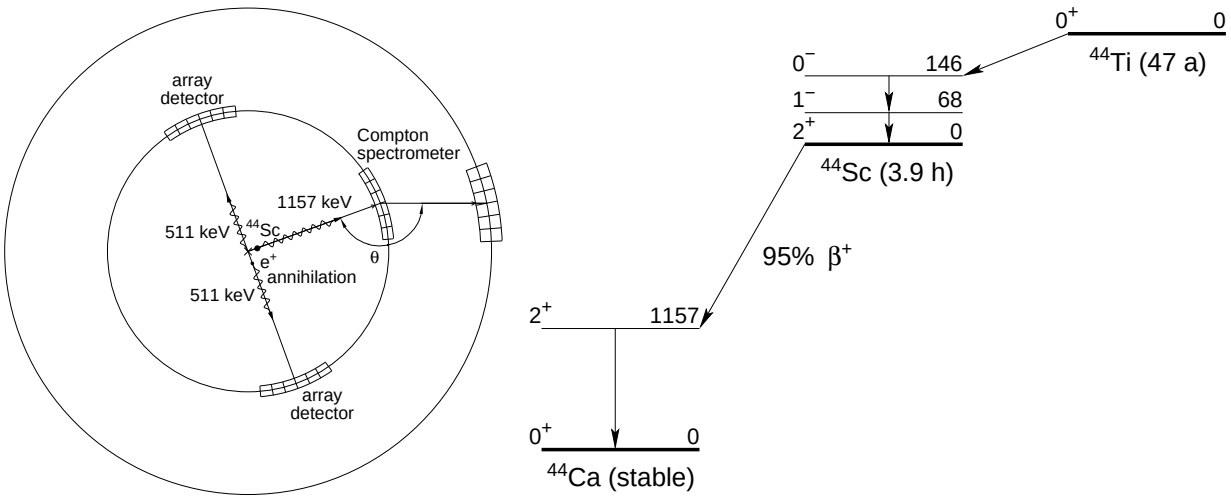

Figure 7. Schematic picture for the combined γ-PET and the ^{44}Ti/^{44}Sc generator.

technology of PET/CT. The co-registration and the reference frame of CT are very helpful for the interpretation of PET images. CT and PET require a comparable dose. Looking at such images it is very apparent, that a significant improvement in the resolution of PET is highly desirable. ^{44}Sc is the best candidate to supply the two 511 keV annihilation quanta together with a strongly populated 1.157 MeV transition as shown in Fig. 7. By measuring the position and direction of this γ-ray accurately with a Compton spectrometer together with the two 511 keV quanta, the location of the emitting nucleus can be located in 3 dimensions. In conventional PET the two collinear 511 keV quanta only allow to determine a two-dimensional localization on a line of response. Thus a much better spatial resolution can be achieved for the same dose with γ-PET compared to PET. With ^{44}Ti (half-life $T_{1/2}$= 59 a), the production with a very promising generator for ^{44}Sc ($T_{1/2}$= 3.9 h) becomes available with γ beams. Again a much stronger population via the fine structure of the Giant Dipole Resonance (GDR) in the ^{46}Ti(γ,2n)^{44}Ti reaction is expected for the ^{44}Ti core consisting of the doubly magic ^{40}Ca and an α particle. The long halflife of ^{44}Ti requires a large transmutation with an intense γ beam, but on the other hand leads to a very valuable, long-lived generator. The production of ^{44}Ti in the (γ,2n) reaction requires rather large γ energies of 21-24 MeV, and would require an increase of the maximum presently planned γ energy at ELI-NP of 19 MeV. This seems possible, since an increase of the electron beam energy by 10% should be achievable after some experience with the accelerator cavities.

4.2.3 γ-PET

The Medium Energy Gamma-ray Astronomy library (MEGAlib)[27] contains all software tools to perform simulations for Compton cameras.[24,26] Similar to measurements in PET detectors, we are including here the detector positions of the coincident 511 keV γ-rays emitted back-to-back in order to determine their common direction. Then we combine this direction of the two 511 keV quanta with the direction of the Compton cone of the 1157 keV quantum. Here are to possiblities of a Compton camera. In the first method we only measure the energy of the Compton scattered electron in the detector together with the direction and energy of the scattered γ ray and obtain by energy considerations the Compton cone as possible directions of the primary γ ray. In a more refind measurement we can measure the momentum of the Compton electron, we measure also its direction. Then we can limit the direction of the primary γ photon to a small section of the Compton cone. We reach accuracies for the primary γ ray of about 1^0. In this way we can filter out on an event-by-event basis the good events, where the reconstruction of the 3D decay location is restricted very much. For the lower energy 511 keV quanta we probably only can reconstruct their Compton cones to determine some Compton scattering in the patient, while for the 1257 keV γ photons we can measure the Compton electron momentum. This reconstruction of the source is very different from the usual PET reconstruction, where the lines of different annihilation decays are combined to reconstruct the source position. If one or more of the three γ quanta (511 keV, 511 keV, 1157 keV) undergo a Compton scattering in the patient, they are strongly suppressed by the analysis including the algorithmus of

the Compton camera, reducing the blurring of the usual PET-analysis by this Compton scattering within the patient strongly. While the diffusion of the positron with a maximum energy of 2 MeV results in a deviation in the annihilation position from the original ^{44}Sc decay, the prompt 1157 keV photon originates from the ^{44}Sc decay. In detailed simulations we want to determine in how far the γ-PET technique results in a strong dose reduction and improved spatial resolution compared to the classical PET analysis.

This γ-PET imaging techniques can be tested with a ^{22}Na source, where the β^+ decay again leads predominantly (in about 90%) to the 2^+-level of ^{22}Ne at 1274.6 keV. However, the long lifetime of ^{22}Na of 2.6 a allows no use in medicine.

5. CONCLUSION

Many further new interesting medical radioisotpes can be produced (see Ref.[1]): new 'matched pairs' of isotopes of the same element become available, one for diagnostics, the other for therapy, allowing to contol and optimize the transport of the isotope by a bioconjugate to the tumor. Also new therapy isotopes become available like ^{225}Ac, where four consecutive α decays can cause much more DNA double-strand breaking. Developing these techniques and applications is a promising task of ELI-NP with a strong societal component.

Acknowlegdement We thank A. Zoglauer, G. Kanbach and R. Diehl to set started with the MEGAlib code package for simulating Compton cameras. We thank A. Tonchev for helping us with the TALYS simulations.

REFERENCES

1. D. Habs and U. Köster, *Production of Medical Radioisotopes with High Specific Activity in Photonuclear Reactions with γ Beams of High Intensity and Large Brilliance*, arXiv-1008.5336v2[physics.med-ph]2010, accepted by Appl. Phys. B, DOI 10.1007/S00340-010-4278-1
2. Ch. Schiepers, *Diagnostic Nuclear Medicine*, Springer Verlag, Berlin (2006).
3. G.J.R. Cook, *Clinical Nuclear Medicine*, Hodder Arnold Publisher, London (2006).
4. J.C. Reubi, H.R. Mäcke, E.P. Krenning, *Candidates for Peptide Receptor Radiotherapy Today and in the Future*, J. Nucl. Med. **46**, 67S (2005).
5. S.A. Jacobs, Comm. Oncology, **7**, 7 (2010).
6. C.A. Boswell and M.W. Brechbiel, *Development of radioimmunotherapeutic and diagnostic antibodies: an inside-out view*, Nucl. Med. Biology **34**, 757 (2007).
7. C.G. Schroer and B. Lengeler, Phys. Rev. Lett. **94**, 054802 (2005).
8. C.G. Schroer et al., Act. Ohys. Pol. A **117**, 357 (2010).
9. B.X. Yang, NIM A, **328**, 578 (1993).
10. A. Snigirev et al., Appl. Opt. **37**, 653 (1998).
11. H.R. Weller, M.W. Ahmed, H. Gao, W. Torrow, U.K. Wu, M. Gai, R. Miskimen, *Research opportunities at the upgraded HIγS facility*, Prog. Part. Nucl. Phys. **62**, 257 (2009).
12. C.P.J. Barty, *Development of Mega-Ray technology at LLNL*, http://www.eli-np.ro/documents/eli-excom-meeting/Barty-100412-ELI-NP-LLNL-MEGa-ray-Intro.pdf (2010).
13. ELI-NP http://www.eli-np.ro/
14. R. Hajima, N. Nakamura, S. Sakanage, Y. Kobayashi, *Design study of the compact ERL*, KEK-Report 2007-7, JAEA-Research 2008-032 (2008).
15. T. Hayakawa, N. Kikuzawa, R. Hajima, T. Shizuma, N. Nishimori, M. Fujiwara M. Seya, *Nondestructive assay of plutonium and minor actinides in spent fuel using nuclear resonance fluorescence with laser compton scattering [gamma]-rays*, Nucl. Instr. Meth. **A 621**, 695 (2010).
16. D.H. Bilderback, J.D. Brock, D.S. Dale, K.D. Finkelstein, M.A. Pfeifer, and S.M. Gruner, *Energy recovery linac (erl) coherent hard x-ray sources*, New Journal of Physics **12**, 035011 (2010), http://stacks.iop.org/1367-2630/12/i=3/a=035011.
17. D.H. Bilderback, G. Hoffstaetter, S.M. Gruner, *R&d towards an energy recovery linac at synchrotron light sources*, Synchrotron Radiation News **6**, 32 (2010).

18. M. Liepe, S. Belomestnykh, E. Chojnacki, Z. Conway, G. Hoffstaetter, R. Kaplan, S. Posen, P. Quigley, J. Sears, V. Shemelin, V. Veshcherevich, *Latest results and test plans from the 100 mA Cornell ERL injector SCRF cryomodule*, Proceedings of IPAC 10, Kyoto, Japan, May 23-28, 2010, http://accelconf.web.cern.ch/AccelConf/IPAC10/papers/wepec066.pdf
19. A. Jankowiak, M. Abo-Bakr, W. Anders, T. Kamps, J. Knobloch, B. Kuske, O. Kugeler, A. Matveenko, A. Meseck, A. Neumann, T. Quast, J. Rudolph, *BERLinPro - a compact demonstrator ERL for high current and low emittance beams*, Proceedings of LINAC 10, Tsukuba, Japan, Sept. 12-17, 2010, to appear. on http://www.JACoW.org/.
20. N.V. Zamfir et al., Phys. Lett. **B 226** 11 (1989).
21. I. Ahmad and P.A. Butler, Ann. Rev. Nucl. and Part. Science, **43** 71 (1993).
22. M. Pruszynski et al., Applied Rad. and Isot. **68**, 1638 (2010).
23. D.V. Filosofov et al., Radiochim. Acta **99**, 149 (2010).
24. M. Frandes et al., IEEE Trans. on Nucl. Science, **57**, 144 (2010).
25. C. Grignon, J. Barbet, M. Bardies, T. Carlier, J.F. Chantal, O. Couturier, J.P. Cassonneau, A. Faivre, L. Ferrer, S. Gireault, T. Haruyama, P. Le Ray, L. Luquin, S. Lupone, C. Metivier, E. Morteau, N. Servagent, D. Thers, *Nuclear medical imaging using $\beta^+\gamma$ coincidences from ^{44}Sc radionuclide with liquid xenon as detector medium*, Nucl. Instr. Meth. **A 571**, 142 (2007).
26. G. Kanbach et al., Nucl. Instr. Meth. A **541**, 310 (2005).
27. MEGAlib software package;http:/www.mpe.de/MEGA/megalib.html
28. J.J. Carroll, M.J. Byrd, D.G. Richmond, T.W. Sinor, K.N. Taylor, W.L. Hodge, Y. Paiss, C.D. Eberhard, J.A. Anderson, C.B. Collins, E.C. Scasbrough, P.P. Antich, F.J. Agee, D. Davis, G.A. Huttlin, K.G Kerris, M.S. Litz, D.A. Whittaker, *Photoexcitation of nuclear isomers by (γ, γ') reactions*, Phys. Rev. **C 43**, 1238 (1991).
29. J.A. Dowell, A.R. Sancho, D. Anand, W. Wolf, *Noninvasive measurements for studying the tumoral pharmacokinetics of platinum anticancer drugs in solid tumors*, Adv. Drug Deliv. Rev. **41**, 111 (2000).
30. A. Bishayee, D.V. Rao, S.C. Srivastava, L.G. Bouchet, W.E. Bolch, R.W. Howell, *Marrow-Sparing Effects of $^{117m}Sn(4+)$Diethylenetriaminepentaacetic Acid for Radionuclide Therapy of Bone Cancer*, J. Nucl. Med. **41**, 2043 (2000).
31. B. Ponsard, S.C. Srivastava, L.F. Mausner, F.F.(Russ) Knapp, M.A. Garland, S. Mirzadeh, *Production of Sn-117m in the BR2 high-flux reactor*, Appl. Radiat. Isot. **67**, 1158 (2009).
32. F. Buchegger, F. Perillo-Adamer, Y.M. Dupertuis, A. Bischof Delaloye, *Auger radiation targeted into DNA: a therapy perspective*, Eur. J. Nucl. Med. **33**, 1352 (2006).
33. M. Guttormsen et al., Phys. Rev **C 83** 014312 (2011).